Proceedings of AJTEC 2011
8th ASME-JSME Thermal Engineering Joint Conference
March 13–17, 2011, Honolulu, Hawaii, USA

AJTEC2011-44341

DRAFT: PHONON TRANSPORT IN ASYMMETRIC SAWTOOTH NANOWIRES

N.A. Roberts and D.G. Walker*
Department of Mechanical Engineering
Vanderbilt University
Nashville, TN USA, 37235

ABSTRACT

Thermal transport in asymmetric sawtooth nanowires was investigated. The boundaries reflect phonons differently depending on the frequency and momentum of the phonon. These systems show thermally rectifying behavior when the boundary reflections are a function of both the direction the phonon is traveling and the frequency of the phonon. This rectifying effect could be useful for thermal management applications at all size scales, but would have to be built up from the nanoscale because of a strong dependence on the device aspect ratio and the Knudsen number of the system. Monte Carlo simulations show an accumulation of phonons at the boundary which emits phonons in a perceived rough direction where those phonons have some probability of diffuse reflections at the boundary while phonons emitted in the smooth direction only experience specular reflections at the boundary and are eventually thermalized at the opposite boundary. In this study the level of rectification of the system was linearly dependent on the device aspect ratio as long as the length of the device was near or below the phonon mean free path of the phonons.

NOMENCLATURE

B scattering constants
D density of states (1/J-m^3)
E energy (J)
F normalized density function
$\mathcal{F}$ exchange factor
k wave vector (1/m)
k_b Boltzmann constant
l device length (m)
N phonon number
$\langle n \rangle$ Bose-Einstein distribution
p probability
R random number
T temperature (K)
t time (s)
V_g phonon group velocity (m/s)
w device width (m)
α aspect ratio (l/w)
η characteristic roughness (m)
ε level of rectification
κ thermal conductivity (W/m-K)
λ phonon wavelength (m)
τ relaxation time (1/s)
ω phonon frequency (Hz)

INTRODUCTION

Thermal rectification is a phenomenon where transport through a material or device is dependent on the sign of the applied temperature gradient or heat current along a specific axis. Reports of this phenomenon date back to 1936 when Starr observed a system consisting of an interface between copper and copperous oxide exhibited both electrical and thermal rectification [1]. In the 1960s and 70s there was a surge of interest in the area of thermal rectification when studies were being performed on composite systems for aerospace applications and additional mechanisms of thermal rectification were discovered. These mechanisms are summarized in ref. [2]. After this explosion of research in the area followed a period of little work

*Address all correspondence to this author.

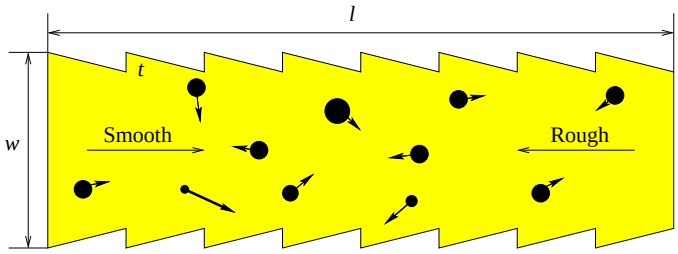

Figure 1. Schematic of the system with direction- and frequency-dependent boundaries

until 2002 when Terraneo et al. developed a model for a 1D nonlinear lattice that could produce rectifying effects [3]. The work by Terraneo et al. caught the attention of many and started a second explosion in thermal rectification research. Since their work in 2002 there have been increasing numbers of papers published on thermal rectification, most of these involve the use of our improved ability to manipulate materials at the nanoscale to enhance the level of the rectifying effect. In 2006 Chang et al. performed measurements on nanotubes that were externally mass loaded with another molecule and observed a rectifying effect where the difference in the directional thermal conductivities of the tube were measured up to 7% [4]. Many theoretical studies have been performed to develop a better understanding of the measurements by Chang et al. and to develop better rectifying systems using asymmetries at the nanoscale [5–20].

In this work we use Monte Carlo simulations to investigate phonon transport in a system with direction- and frequency-dependent boundaries. These boundaries can be thought of as an asymmetric sawtooth structure as shown in Figure 1 where the characteristic roughness of the sawtooth feature, t is of the order of the dominant phonon wavelength. This work was motivated by the work of Saha et al. [21] and Moore et al. [22] where they performed Monte Carlo simulations of phonon backscattering in nanowires with sawtooth boundary roughness. We will study the impact of the device aspect ratio, device temperature and the size of the asymmetric feature on the level of rectification and level of self biasing.

ANALYSIS

To study boundaries as a possible mechanism for thermal rectification we use a Monte Carlo (MC) method to simulate phonon transport. To perform these simulations we must first determine the number of phonons to be initialize in the system. This calculation is performed by summing the number of phonons in each of the 1000 discrete frequency ranges by

$$N(p) = \sum_{i=1}^{N_b} \langle n(\omega_{0,i}, p)\rangle D(\omega_{0,i}, p)\Delta\omega_i. \tag{1}$$

This results in a very large number of phonons which is not realistic to simulate with current computational capabilities. Because of this limitation on the number of phonons we are capable of simulating, we prescribe a set number (100,000) and calculate a scaling factor given by

$$W = \frac{N_{actual}}{N_{prescribed}}. \tag{2}$$

This scaling factor will be used in the remaining calculations. The location of each phonon is obtained from a uniform distribution in all three dimensions. To obtain the frequency of the phonon, the normalized cumulative number density function is used from [23]

$$F(\omega) = \sum_b \frac{\int_0^{\omega}\langle n\rangle D(\omega)d\omega}{\int_0^{\omega_{\max,b}}\langle n\rangle D(\omega)d\omega}, \tag{3}$$

where $\langle n\rangle$ is the Bose-Einstein distribution given by [24]

$$\langle n\rangle = \frac{1}{\exp\left[\frac{\hbar\omega}{k_B T}\right] - 1} \tag{4}$$

and $D(\omega)$ is the 3-D density of states given by

$$D(\omega) = \frac{k^2}{2\pi^2 V_g}, \tag{5}$$

where k is given by the inverse dispersion relation

$$k = \frac{\arccos\left[1 - \frac{2\omega^2}{\omega_{\max,b}^2}\right]}{a}. \tag{6}$$

Here b is the branch (LA or TA), a is the lattice constant and $\omega_{\max,b}$ are the maximum phonon frequencies for the longitudinal and transverse acoustic branches which are 1.23×10^{13} Hz and 4.5×10^{12} Hz, respectively. A random number is drawn and the frequency range is determined for that phonon by finding where the random number falls within the 1000 spectral intervals in the cumulative number density function. The interval is determined by applying $F_{i-1} < R < F_i$. Upon determining the spectral interval, the phonon frequency is calculated using

$$\omega = \omega_{0,i} + (2R-1)\frac{\Delta\omega_i}{2}, \tag{7}$$

where R is the same random number used to determine the spectral interval. The polarization of the phonon is then determined next by calculating the probability of LA to TA phonons in the ith spectral interval. The probability of the phonon being in the LA branch is given by [23]

$$P_i(LA/TA) = \frac{N_i(LA)}{N_i(LA)+N_i(TA)}, \tag{8}$$

where N_i is the unsummed portion of equation 1. A random number is again selected and compared to $P_i(LA)$ to determine the polarization. The individual components of momentum are calculated using

$$k_x = k\sin\theta\cos\psi \tag{9}$$

$$k_y = k\sin\theta\sin\psi \tag{10}$$

$$k_z = k\cos\theta \tag{11}$$

where k is the total isotropic momentum. The directions $\cos\theta = 2R_1 - 1$ and $\psi = 2\pi R_2$, which are the polar and azimuthal angles, are chosen from uniformly distributed random numbers, R_1 and R_2, which range from zero to one. In this work we assume an analytic dispersion given by

$$\omega_b(k) = \omega_{\max,b}\sqrt{\frac{1-\cos ka}{2}}. \tag{12}$$

Because the model does not consider realistic dispersions and anisotropy, the results will not compare directly to a specific device. Instead we are looking for trends and order of magnitude of effects. We have also chosen to neglect optical phonons because of their minimal contribution to the thermal transport due to their small group velocity [24].

After phonons are initialized they are allowed to drift linearly based on their individual momenta for a prescribed time step of 1 ps. The simulations are run long enough to achieve steady state solutions. If a phonon crosses an adiabatic boundary during the drift phase it is backed up to the first boundary it strikes and is reflected. The reflection of the phonon is dependent on the sign of the x-component of momentum (k_x) and its frequency. If a phonon has a positive k_x it will always reflect specularly because it only sees the smooth surface, but if a phonon has a negative k_x then a scattering parameter p is calculated, which is given by equation 22. A random number (R) is generated and compared to p, if $p > R$ the phonon is reflected specularly, otherwise it is reflected diffusely. For diffuse reflection the individual components of momentum are recalculated with the same total momentum and frequency in order to conserve energy. The phonon is then allowed to drift for the remainder of the time step. After each time step the energy, number of phonons and average temperatures of each of the cells is calculated.

The simulations have been designed for two boundary conditions for the boundaries that have no direction- or frequency-dependence. The first is an adiabatic condition in which all phonon reflect specularly when they interact with the boundary. The second is a constant temperature boundary condition in which all phonons that interact with the boundary are thermalized and at each time step a specified number of phonons are emitted with there statistics coming from an equilibrium distribution at the specified boundary condition.

To recover solutions of diffuse or continuum thermal transport we must also include a scattering model for three-phonon scattering. In this work we have used the scattering model presented by Holland for silicon [25]. The first step in determining if a phonon scattered during the drift phase is to calculate the relaxation times for the various three-phonon scattering processes

$$\frac{1}{\tau_{NU}} = B_L\omega^2T^3(LA,\text{Normal+Umklapp}), \tag{13}$$

$$\frac{1}{\tau_N} = B_{TN}\omega T^4(TA,\text{Normal}), \tag{14}$$

$$\frac{1}{\tau_U} = 0(TA,\text{ Umklapp for } \omega < \omega_{1/2}), \tag{15}$$

$$\frac{1}{\tau_U} = B_{TU}\omega^2/\sinh\left(\frac{\hbar\omega}{k_bT}\right)(TA,\text{ Umklapp for } \omega > \omega_{1/2}), \tag{16}$$

where $\omega_{1/2}$ is the frequency corresponding to $k/k_{\max} = 0.5$. The constants in these equations are taken from Holland [25]

$$B_L = 2.0\times10^{-24}\text{s/deg}^3, \tag{17}$$

$$B_{TN} = 9.3\times10^{-13}1/\text{deg}^3, \tag{18}$$

$$B_{TU} = 5.5 \times 10^{-18}\text{s}. \tag{19}$$

The overall relaxation time is then calculated using

$$\frac{1}{\tau_{NU}} = \frac{1}{\tau_N} + \frac{1}{\tau_U}. \tag{20}$$

The probability of that phonon scattering is then calculated using

$$P_{NU} = 1 - \exp(-\Delta t/\tau_{NU}), \tag{21}$$

where Δt is the time step in the simulation (1 ps). A random number is then generated and compared to the probability of scattering. If the probability of scattering is greater than the random number the phonon is scattered which resets that phonon's frequency, wave-vector and polarization from the equilibrium distribution at the temperature of the cell the phonon is located. Following the scattering, an energy balance scheme is implemented which forces conservation of energy of the system by adding or subtracting phonons until energy if conserved. When a phonon is added during this phase it is also pulled from the equilibrium distribution at the cell temperature. This balance scheme and the scattering scheme are performed to drive the cell towards local thermodynamic equilibrium which is the role of three-phonon scattering.

In this work we studied devices aspect ratios from 0.01 to 10 where we define the aspect ratio as the length over the width of the device. We also varied the roughness of the surface seen by the left-moving phonons with values of $\eta = 0$ to 1×10^{-9}m where the probability of a diffuse reflection from the boundary is given by

$$p(\omega, \eta) = \exp\left[-\frac{64\pi^5\eta^2\omega^2}{V_g^2}\right]. \tag{22}$$

From equation 22, the probability of reflecting specularly decreases as the roughness and phonon frequency increases.

A median frequency between specular and diffuse reflections for the left-moving phonons can be obtained by setting $p = 0.5$ and then calculating the frequency as a function of the characteristic surface roughness as in equation 22. This frequency is the median frequency for which frequencies less than it will reflect specularly and frequencies greater than it will reflect diffusely on average. The cumulative density function in Figure 2 is the fraction of phonons that exist at or below a particular frequency for a given temperature. This distribution shows that below a specified frequency there is a higher density of low frequency phonons for lower temperatures. With knowledge of the median frequency along with the cumulative density function

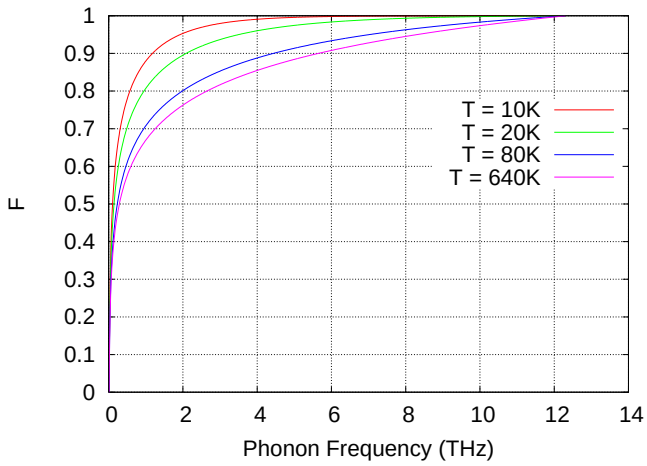

Figure 2. Cumulative phonon density function versus frequency at various temperatures

at a specific temperature one can approximate the level of self-biasing of the device. The level of self-biasing in this work is determined by the device's ability to force a non-uniform temperature distribution with no externally applied heat flux similar to what happens electrically in a *pn*-junction.

To determine the magnitude of the rectifying effect we define a level of rectification using

$$\varepsilon = \frac{\kappa^+ - \kappa^-}{\kappa^+ + \kappa^-}, \tag{23}$$

where κ is the thermal conductivity and $^+$ and $^-$ represent the forward and reverse conduction directions. This definition of the level of rectification will result in a value of zero when there is no difference in the directional thermal conductivities, ie. no rectification, and a value of one for an ideal rectifier in which either one conductivity is infinite or zero.

RESULTS

In this section the results of the simulations of direction- and frequency-dependent boundaries are presented and discussed based on the system parameters. We focus on the impact of device aspect ratio, device temperature and the surface roughness in the rough direction.

Effects of Device Aspect Ratio

The device aspect ratio plays an extremely important role in both the level of rectification and self-biasing of the device. When device aspect ratios are small the direction- and frequency-dependent boundaries are expected to result in little to no significant rectification or biasing because of the smaller relative im-

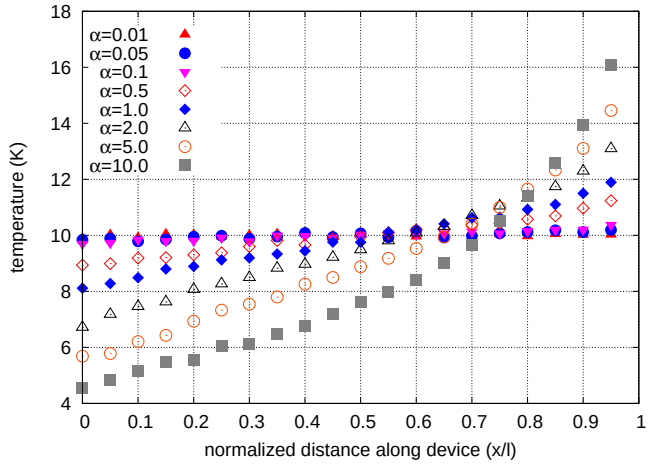

Figure 3. Temperature distribution for devices of varying aspect ratio with adiabatic boundary conditions and direction- and frequency dependent boundary scattering

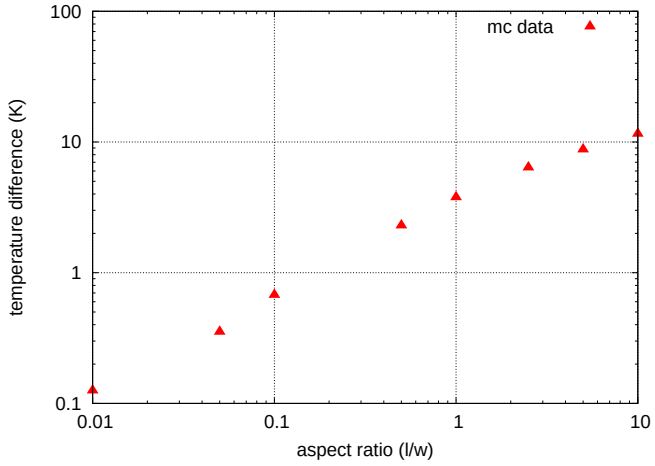

Figure 4. Temperature difference between device ends as a function of device aspect ratio

pact of the boundaries on the thermal transport. Figure 3 shows temperature distribution of devices simulated with different aspect ratios with adiabatic boundaries. This portion of the work was performed in the ballistic transport regime in order to eliminate any effects due to three-phonon scattering. In this figure we can see that as the aspect ratio increases ($\alpha = \frac{l}{w}$) the resulting temperature distribution becomes less and less uniform. These results show that as the aspect ratio increases or the length of the device increases with respect to the other dimensions the impact of the boundaries become greater. In this case we have force the condition of completely specular boundary reflections in the smooth direction (left to right) and completely diffuse boundary reflections in the rough direction (right to left) to show the maximum level of biasing possible in the device. Figure 4 shows the difference in the boundary temperatures as a function of the device aspect ratio. We clearly see from this figure that the level of self-biasing increases with device aspect ratio. The reason we see a non-uniform temperature distribution in a case were we should not is because the direction- and frequency-dependent boundaries break the symmetry of the system which we have already determined to be a requirement for thermal rectification. These boundaries act as a filter and only allow low frequency phonons to travel in the rough direction if they strike a boundary while all phonons travel freely in the smooth direction. This filtering effect is increased with device aspect ratio because the device is becoming longer and narrower increasing the probability that a phonon will interact with the boundary. The increased interaction with the boundary means that phonons moving in the rough direction will have a decreased probability in traversing the device and will likely be diffusely scattered at the right end of the device.

To investigate the impact of aspect ratio on thermal rectification we must apply thermalizing boundaries to impose an external temperature gradient across the device. We calculate the resulting heat current across the system by collecting the energy absorbed and emitted by each boundary over the entire simulation once reaching steady state. Figure 5 shows the level of rectification defined in equation 23 as a function of the aspect ratio. The level of rectification increases dramatically with the aspect ratio of the device where we see at device of aspect ratio of 10 ($l = 10w$) has a level of rectification of about 95. In the low aspect ratio range (under about 1) we see a roughly linear trend in the level of rectification with device aspect ratio. In the region of device aspect ratios greater than this we see a greater than linear trend. This relationship could result in large levels of rectification if these boundaries could be created in a nanowire or nanotube which are extremely high aspect ratio devices. An additional feature to note here is that the effective thermal conductivity of the smooth direction does not decrease with increasing device aspect ratio, but actually increases because of the contribution of some of the diffusely scattered phonons that were initially traveling in the rough direction. Figure 6 shows the effective rectification in each direction of the device as a function of the device aspect ratio. This is an important feature because the device maintains good conductivity properties in one direction and an insulating behavior in the opposite.

The non-equilibrium is clearly enhanced with increasing device aspect ratio, which is seen as larger differences in the temperature distributions in the adiabatic cases. In these simulations the phonons collect near the right boundary. Realize that temperature is an equilibrium quantity, and this system is not in equilibrium. Therefore the temperature represents an average energy weighted by the distribution of phonon frequencies.

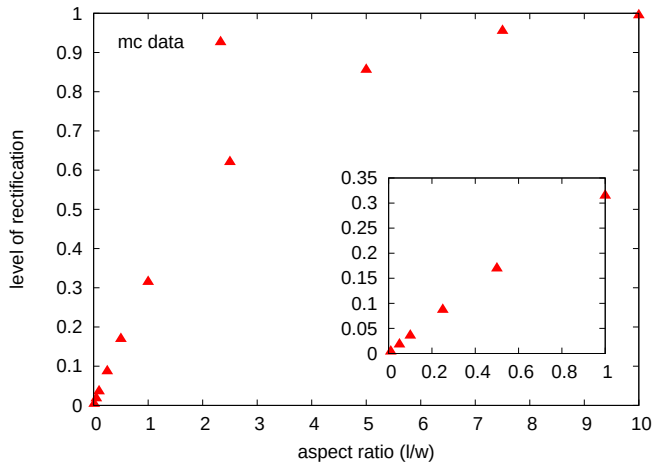

Figure 5. Level of rectification as a function of device aspect ratio

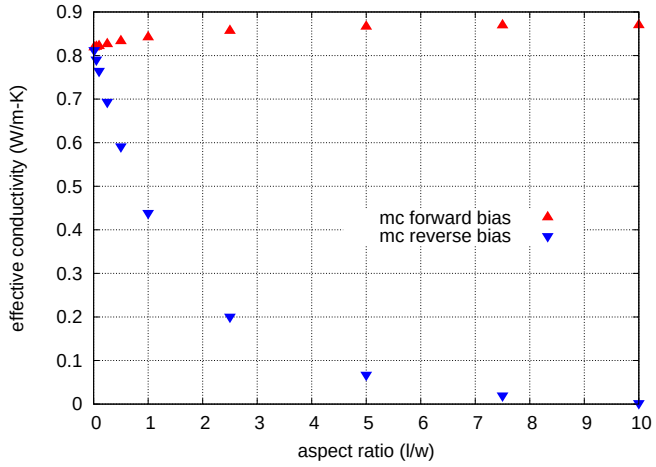

Figure 6. Effective thermal conductivity in each direction of the device as a function of device aspect ratio

Effects of Temperature

The temperature of the device plays an important role even beyond that of three-phonon scattering, where scattering rates increase with temperature [25]. At higher temperatures the cumulative density function (Figure 2) tells us that there is a higher concentration of high frequency phonons than at lower temperatures. Since the probability of a diffuse boundary scattering event in the Monte Carlo simulations is increased with increasing frequency, as defined by p in equation 22, we expect that the amount of self-biasing in the unbiased device with direction- and frequency-dependent boundaries also increases with temperature until three-phonon scattering eliminates the effect of the boundaries. The increase in biasing with temperature is a result of the higher frequency phonons being trapped near the right boundary because of their high probability of a diffuse scattering

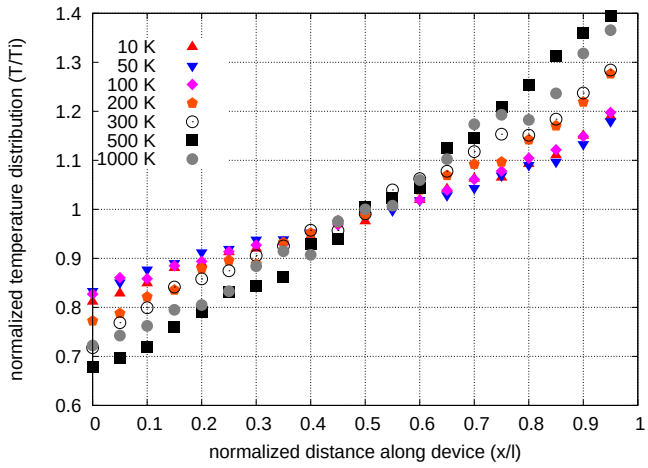

Figure 7. Normalized temperature distribution through asymmetric and frequency dependent boundary device for various temperatures using Monte Carlo simulation

event when striking a boundary while moving in the rough direction. Figure 7 confirms our hypothesis by showing the normalized temperature distribution through the unbiased device from 10 K to 1000 K for a fixed aspect ratio and surface roughness, where each temperature distribution is normalized by the initially prescribed temperature of the device. At low temperatures we see little impact from increasing initial temperature of the device because there is little difference in the phonon frequency distribution at these temperatures. As we increase the temperature to higher temperature we see an increase in the normalized temperature distribution across the device because of the greater concentration of high frequency phonons that have a higher probability of diffuse reflections than the lower frequency phonons. At even higher temperatures we begin to see a reduction in the biasing of the device because of three-phonon scattering occurring at a high rate. If we were able to simulate a device at extremely high temperatures we would eventually see no biasing because the mean free path of the phonons would become so small the occasional diffuse reflection from the boundary would not be observed. In Figure 8 we have calculated the difference of the temperatures of the devices near the right and left boundaries and plotted them as a function of the initial device temperature. In this figure we see the same result as before, but without the clutter of many data points.

Again we are more interested in the rectifying effects when a heat current or temperature gradient is applied. Figure 9 shows the level of rectification as a function of the average temperature of the device between two constant temperature baths at different temperatures. We clearly see an increasing of the rectifying effect in this temperature range. If we go to higher temperatures we will again see a reduction due to high levels of three-phonon scattering. In Figure 10 we have plotted the effective thermal

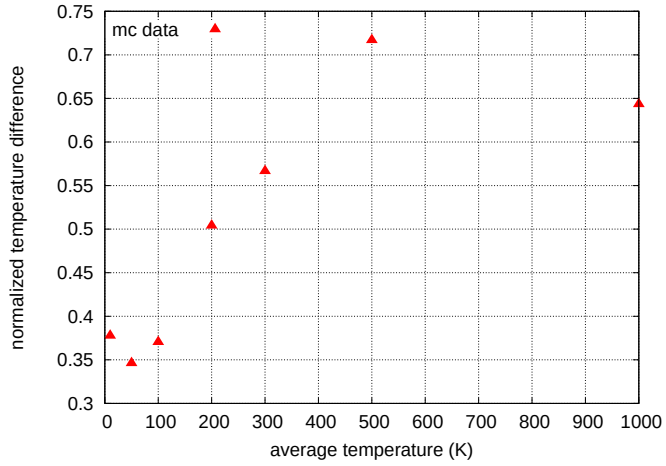

Figure 8. Normalized temperature difference between the right and left boundaries of a device with direction- and frequency-dependent boundaries with all adiabatic boundary conditions as a function of the initial device temperature

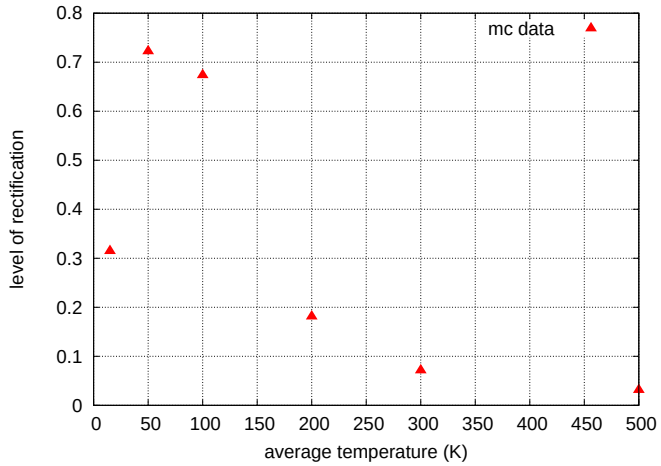

Figure 9. Level of rectification as a function of the average device temperature between two constant temperature baths at different temperatures

conductivity as a function of temperature gradient direction and the average device temperature.

Effects of Boundary Roughness

Surface roughness of the boundaries also has an impact on the self-biasing. If a device was designed with only a directional-dependence and no frequency-dependence (from the difference in surface roughness) no self-biasing would be observed. This is shown by using MONT2D, which is an independent Monte Carlo code used to calculate radiation exchange factors [26]. The results of this analysis are shown in Table 1. Because the shape factors are similar for alternating directions the amount of rectification can be considered negligible.

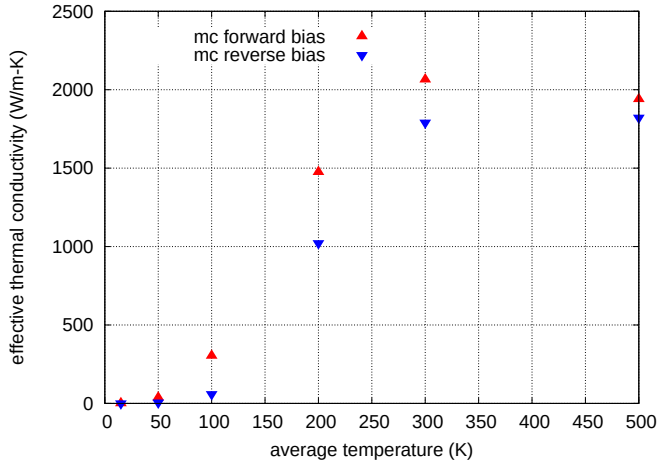

Figure 10. Effective thermal conductivity as a function of direction and average device temperature

Table 1. Radiation exchange factors for configuration shown in Figure 1. The difference in the exchange factors represents the amount of rectification. The three surfaces of the sawtooth structure are specular (S) or diffuse (D). The percent difference between $\mathcal{F}_{12}$ and $\mathcal{F}_{21}$ associated with the tooth height $t = 1.8$ is 6.06×10^{-4} and that associated with $t = 0.2$ is 9.83×10^{-4}. Therefore, no configuration exhibits rectification.

$t = 1.8$			$t = 0.2$		
Surface	$\mathcal{F}_{12}$	$\mathcal{F}_{21}$	Surface	$\mathcal{F}_{12}$	$\mathcal{F}_{21}$
SSS	0.09675	0.09609	SSS	0.82446	0.82547
DDD	0.09550	0.09551	DDD	0.65363	0.65481
DSD	0.09656	0.09880	DSD	0.65836	0.65790
SDS	0.09751	0.09591	SDS	0.83013	0.83205

When the difference in roughness is introduced a resulting frequency dependence is also introduced as defined by p, from equation 22. Figure 11 shows the self-biasing as a function of the surface roughness for different aspect ratios. As the surface roughness is increased the biasing also increases due to the increased diffuse scattering events by left-moving phonons. The increase in surface roughness effectively reduces the cutoff frequency therefore increasing the probability of diffuse scattering events as defined by p.

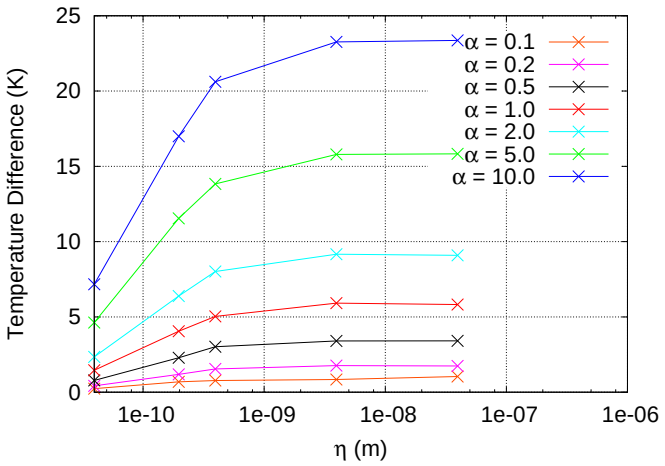

Figure 11. Temperature difference as a function surface roughnesses in the rough direction for several aspect ratios

CONCLUSIONS

This work has shown how asymmetric nanostructures which possess directional- and frequency-dependent boundaries can result in thermally self-biasing as well as thermally rectifying behavior. For biasing and rectification to occur both of these properties must be present which is an important factor to consider in the design of a device of this nature. For a device like this to function with high levels of rectification the device temperature must be kept low to minimize three-phonon scattering. To this point little attention has been paid to the method for fabricating and testing a device like this other than the schematic found in the introductory chapter of this document. In order to have a device that produces thermal rectification the smooth direction must be nearly atomically smooth so that the majority of phonon reflections are specular.

REFERENCES

[1] Starr, C., 1935. "The copper oxide rectifier". *Physics (Journal of Applied Physics)*, **7**, Jan., pp. 15–19.

[2] Roberts, N., and Walker, D., 2010. "Thermal rectification in solid materials". *in preparation*.

[3] Terraneo, M., Peyrard, M., and Casati, G., 2002. "Controlling the energy flow in non-linear lattices: A model for a thermal rectifier". *Physical Review Letters*, **88**(9), Mar., pp. 4302.1–4302.4.

[4] Chang, C. W., Okawa, D., Majumdar, A., and Zettl, A., 2006. "Solid-state thermal rectifier". *Science*, **314**, Nov., pp. 1121–1124.

[5] Alaghemandi, M., Algaer, E., Bohm, M., and Muller-Plathe, F., 2009. "The thermal conductivity and thermal rectification of carbon nanotubes studied using reverse non-equilibrium molecular dynamics simulations". *Nanotechnology*, **20**(115704), feb.

[6] Alaghemandi, M., Leroy, F., Algaer, E., Bohm, M., and Muller-Plathe, F., 2010. "Thermal rectification in mass-graded nanotubes: a model approach in the framework of reverse non-equilibrium molecular dynamics simulations". *Nanotechnology*, **21**(075704).

[7] Roberts, N., and Walker, D., 2008. "Monte Carlo study of thermal transport of direction and frequency dependent boundaries in high Kn systems". In Proceedings of ITherm 2008.

[8] Miller, J., Jang, W., and Dames, C., 2008. "Thermal rectification by ballistic phonons". In Proceedings of 3rd Energy Nanotechnology International Conference.

[9] Miller, J., Jang, W., and Dames, C., 2009. "Thermal rectification by ballistic phonons in asymmetric nanostructures". In Proceedings of the ASME 2009 Heat Transfer Summer Conference.

[10] Wu, G., and Li, B., 2007. "Thermal rectification in carbon nanotube intramolecular junctions: Molecular dynamics calculations". *Physical Review B*, **76**(085424), aug.

[11] Wu, G., and Li, B., 2008. "Thermal rectifiers from deformed carbon nanohorns". *Journal of Physics: Condensed Matter*, **20**(175211).

[12] Yang, N., Zhang, G., and Li, B., 2008. "Carbon nanocone: a promising thermal rectifier". *Applied Physics Letters*, **93**(243111).

[13] Yang, N., Zhang, G., and Li, B., 2009. "Thermal rectification in asymmetric graphene ribbons". *Applied Physics Letters*, **95**(033107).

[14] Hu, M., Keblinski, P., and Li, B., 2008. "Thermal rectification at silicon-amorphous polyethylene interface". *Applied Physics Letters*, **92**(211908), may.

[15] Hu, J., Ruan, X., and Chen, Y., 2009. "Thermal conductivity and thermal rectification in graphene nanoribbons: a molecular dynamics study". *Nano Letters*.

[16] Hu, J., Ruan, X., and Chen, Y., 2009. "Molecular dynamics study of thermal rectification in graphene nanoribbons". *International Journal of Thermophysics*.

[17] Hu, M., Goicochea, J., Michel, B., and Poulikakos, D., 2009. "Thermal rectification at water/functionalized silica interfaces". *Applied Physics Letters*, **95**(151903).

[18] Noya, E., Srivastava, D., and Menon, M., 2009. "Heat-pulse rectification in carbon nanotube Y junctions". *Physical Review B*, **79**(115432).

[19] Roberts, N., and Walker, D., 2010. "Computational study of thermal rectification from nanostructured interfaces". *Journal of Heat Transfer, submitted*.

[20] Walker, N. R. D., 2010. "Phonon wave-packet simulations of Ar/Kr interfaces". In ITherm 2010, IEEE.

[21] Saha, S., Shi, L., and Prasher, R., 2006. "Monte Carlo simulation of phonon backscattering in a nanowire". In Pro-

ceedings of the ASME International Mechanical Engineering Congress and Exposition.

[22] Moore, A., Saha, S., Prasher, R., and Shi, L., 2008. "Phonon backscattering and thermal conductivity suppression in sawtooth nanowires". *Applied Physics Letters,* **93**(083112), August.

[23] Mazumder, S., and Majumdar, A., 2001. "Monte carlo study of phonon transport in solid thin films including dispersion and polarization". *Journal of Heat Transfer,* **123**(4), June, pp. 749–759.

[24] Kittel, C., 1986. *Introduction to Solid State Physics*, 6th ed. Wiley, New York.

[25] Holland, M. G., 1963. "Analysis of lattice thermal conductivity". *Physical Review,* **132**(6), Dec., pp. 2461–2471.

[26] Burns, P. J. mont2d. http://www.colostate.edu/ pburns/monte/code.html.